Structural, ferroelectric, and optical properties of Bi3+ doped YFeO3: A first-principles study

E. Martínez-Aguilar[1], H´Linh Hmŏk[2,3,*], J. Ribas-Ariño[4], J.M. Siqueiros Beltrones[5], R.Lozada-Morales[1]

[1]*Benemérita Universidad Autónoma de Puebla, Postgrado en Física Aplicada, Facultad de Ciencias Físico-Matemáticas, Col. San Manuel Ciudad Universitaria, Av. San Claudio y Av. 18 sur, Puebla Pue, CP 72570, Mexico*
[2]*Computational Laboratory for Advanced Materials and Structures, Advanced Institute of Materials Science, Ton Duc Thang University, Ho Chi Minh City, Vietnam*
[3]*Faculty of Applied Sciences, Ton Duc Thang University, Ho Chi Minh City, Vietnam*
[4]*Departament de Ciència de Materials i Química Física and IQTCUB, Universitat de Barcelona, Martí i Franquès 1, 08028 Barcelona, Spain*
[5]*Centro de Nanociencias y Nanotecnología, Universidad Nacional Autónoma de México, AP 14, Ensenada 22860, Baja CA, Mexico*

*Corresponding author e-mail: *hlinh.hmok@tdtu.edu.vn*

Abstract

The orthoferrites with the general formula $RFeO_3$ (R = Ho, Er, Lu, Sc, and Y) have recently attracted a great deal of attention because they are promising candidates for a second generation of multiferroic materials. In this computational work, the structural, ferroelectric and optical properties of the $YFeO_3$ perovskite oxide (YFO) and a Bi-doped $YFeO_3$ were analyzed. Bi-substitution in YFO leads to an increase of its lattice parameters by virtue of the larger ionic radius of Bi^{3+}. Both compounds exhibit a G-type antiferromagnetic ground state. The calculations disclose a significant spontaneous polarization along the [101] direction of YFO-Bi, which originates in the asymmetric distribution of the charges around the Bi^{3+} ions, as a result of the Bi-6s electrons. The electric polarizability of YFO is increased upon Bi^{3+}-doping and the more significant components of the real permittivity tensor of YFO-Bi are those associated with the direction along which the maximum value of spontaneous polarization is observed. The spontaneous polarization of YFO-Bi found in this work reveals that this compound holds the potential for the next generation of multi ferroic materials.

1. Introduction

Bismuth ferrite ($BiFeO_3$) represents the first generation of multiferroic materials with coupled ferroelectric and antiferromagnetic orders at room temperature.[1] But the high leakage current and often accompanying secondary phases such as $Bi_2Fe_4O_9$ have been the prime hurdle for its practical application.[2] Orthoferrites with the general formula $RFeO_3$ (R = Ho, Er, Lu, Sc, and Y) are the second generation of multiferroic materials. These materials are attractive for potential applications in data storage, sensors and communication.[3] The $YFeO_3$ perovskite oxide (space group D2h-Pnma) shows no ferroelectric polarization but is a weak ferromagnet due to a small canting of the antiferromagnetically ordered moments.[4] It presents a magnetic transition at the Neel temperature of 370–C.[5] Many works are focused on the effects of the magnetic properties of $YFeO_3$ upon doping of the A (Y^{3+}) or B (Fe^{3+}) sites with different ions (Ca, Gd, Er, Mn, Ti, $Bi^{).}$[2,6–10] However, there are hardly any reports on their ferro-electric properties. From a theoretical point of view, Zhang et al.[11] studied the effect of Y (6.25%) substitution on the structural and electronic properties of $BiFeO_3$ using density functional theory calculations. They found that the ferroelectric distortion of the $BiFeO_3$ structure with Y^{3+} substitution is significantly affected by the hybridization of substituted d states and oxygen 2p states. However, the electric polarization value was not reported. In a more recent article, using density functional theory (DFT), J. Kaczkowski investigated the ferroelectric properties of $Bi_{1-x}Y_xFeO_3$ and $Bi_{1-x}La_xFeO_3$ solid solutions, where reported that the polarization value of the orthorhombic Pn21a phase decreases monotoni- cally from 3 to 0 $\mu C/cm^2$ for $Bi_{1-x}Y_xFeO_3$, and from 25 to 0 $\mu C/cm2$ for $Bi_{1-x}La_xFeO_3$ with x = 0 to 1.[12] Despite the interesting properties of YFO and doped YFO, there is not any detailed discussion on the ferroelectric properties of YFO doped with Bi^{3+} (YFO-Bi) based on first-principles cal- culations in the literature. For this reason, in this work we investigate the structural, electronic, ferroelectric, and optical properties of YFO-Bi, using density functional theory. Additionally, the spontaneous polarization of YFO-Bi is addressed using the Modern Theory of Polarization via Berry phase approach and calculations of dielectric function are used to determine the optical properties.

2. Computational details

The simulations were carried out in the framework of the standard density functional theory (DFT) in the periodic cell model and plane-wave basic set by using the Quantum-Espresso package.[13] We generated norm-conserving pseudopotentials with the OPIUM package.[14,15] Norm-conserving pseudopotentials with the configurations of $5d^{10}6s^26p^3$ for Bi, $4s^24p^64d^15s^2$ for Y, $3d^64s^2$ for Fe and $2s^22p^4$ for O were used. The exchange correlation effects were described by the generalized gradient approximation (GGA) based on the Perdew-Burke-Ernzerhof (PBE) functional. All calculations were done with a plane wave cutoff energy of 75 Ry and a total energy convergence threshold of 10^{-6} eV. Full relaxation calculations were performed until the convergence threshold for all components of the residual energy and forces was reached 10^{-4} Ry/atom and 10^{-3} Ry/bohr, respectively. Monkhorst-Pack *k*-point $6 \times 4 \times 6$ was used for geometry optimization while the densities of states (DOS) were calculated using a $12 \times 8 \times 12$ *k*-point meshes. Non collinear magnetic solutions were investigated to calculate the magnetic moment, including the Spin-Orbit Coupling (SOC) interaction. The polarization of $YFeO_3$ and YFO-Bi was calculated via Berry phase using the method first developed by King-Smith and Vanderbilt.[16,17] The optical properties of the compounds were determined using the complex dielectric function $\varepsilon(\vec{q},\omega)$ dependent on frequency (ω) and wave vector $\vec{q}$, whose complex elements can be represented as a 3×3 tensor[18]:

$$\varepsilon(\vec{q},\omega)_{\alpha\beta} = \varepsilon_r(\vec{q},\omega)_{\alpha\beta} + i\varepsilon_i(\vec{q},\omega)_{\alpha\beta} \quad (1)$$

where ε_r is the real part and ε_i is the imaginary part of the dielectric function.

$$\varepsilon_i(\vec{q},\omega) = \frac{8\pi^2}{N(2a)^3}\left(\frac{e}{m\omega}\right)^2 \sum_{if}\left|\langle f|e^{i\vec{q}.\vec{r}}\vec{a}_0\cdot\vec{p}|i\rangle\right|^2 \times\delta\left(E_f - E_i - \hbar\omega\right)f(E_i)[1-f(E_f)] \quad (2)$$

Where e is the charge of the electron, $|i\rangle$ is the initial state and $\langle f|$ the final state, E_i and E_f are the corresponding energies, $\vec{p}$ is the dipole matrix. $f(E_i)$ is the probability that the initial state is occupied and $[1 - f(E_f)]$ is the probability that the final state is empty, $\alpha\beta = xy, xz, or\ yz$.

The real part ε_r is determined by ε_i through the Kramers-Kroning dispersion as [18]:

$$\varepsilon_r(\vec{q}, \omega) = 1 + \frac{2}{\pi} P \int_0^{\infty} \frac{\omega' \varepsilon_i(\vec{q},\omega)}{\omega'^2 - \omega^2} d\omega' \quad (3)$$

Here P indicates the main value.

3. Results and discussion

$YFeO_3$ (YFO) has orthorhombic perovskite unit cell (space group No. 62, *Pnma*) with lattice parameters a = 5.5877(3) Å, b = 7.5951(4) Å and c = 5.2743(2) Å, that were taken from Reference [19]. Figure 1 hows the unit cell of YFO and $Y_{0.75}Bi_{0.25}FeO_3$ (YFO-Bi) after structural relaxation. Concerning the YFO-Bi cell, it should be mentioned that four different configurations were initially built (see Figure. S1 in the Supporting Information). All these different configurations have the same energy (see Table S1). For this reason, we will hereafter consider a single configuration, namely the YFO-Bi cell as displayed in Figure 1B (configuration a in Figure S1). The 25% Bi doping of YFO is within the studied range of impurification keeping the orthorhombic structure with space group *D2h-Pnma*.[10-12] There is an increase in the lattice parameters in the YFO-Bi structure with respect to that of the YFO, a = 5.756 Å, b = 7.824 Å and c = 5.433 Å, attributed to the ionic radius of Bi (1.03 Å) being larger than that of Y (0.90 Å).[20] To determine the ground-state magnetic order, we compared the total energies of ferromagnetic (FM) and G-type (AFM-G) antiferromagnetic ordering for both YFO and YFO-Bi. The energy differences, $\Delta E = E_{FM} - E_{AFM}$ is 411 and 796 meV per formula unit for YFO and YFO-Bi, respectively. Therefore, the ground-states of YFO and YFO-Bi are AFM. This result coincides with the experimental works reported

in references 4,10. Here, we have only considered the AFM-G configuration (see Figure 1). In Table S2 in the Supplementary Information, details of the magnetic moments are shown; these values are obtained from the self-consistent calculation, for both YFO and YFO-Bi in their AFM-G configuration. For both systems, the local magnetic moment of the Bi/Y ion is almost zero, since Y^{3+}/Bi^{3+} is strongly diamagnetic.[19,21] The Fe^{3+} ion has a magnetic moment of ±4.03 μB, similar to that reported by the References 22,23.

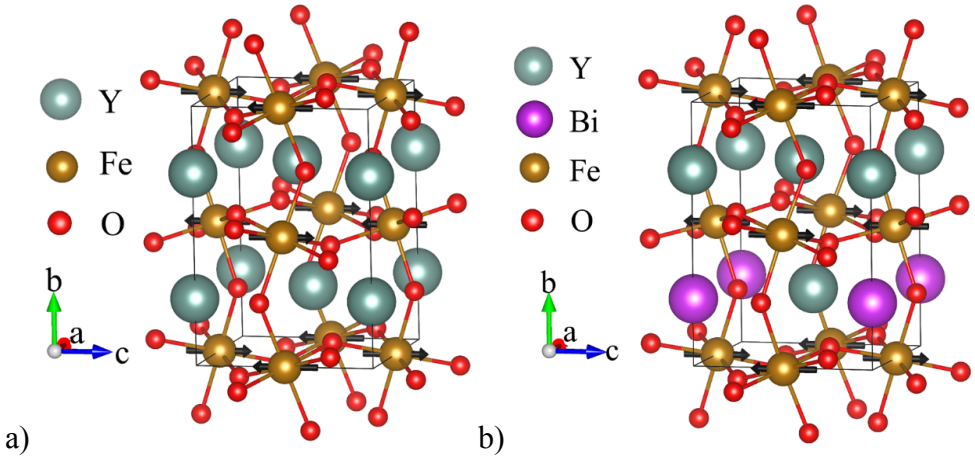

Figure 1. Unit cell of a) $YFeO_3$ and b) $Y_{0.75}Bi_{0.25}FeO_3$ after structural relaxation.

The total density of states (TDOS) and the band structure for the *spin-up* and *spin-down* states of YFO and YFO-Bi are presented in Figures 2A, B respectively. For both cases, the TDOS is completely symmetric; moreover, there are no differences in band structure between the *spin-up* and *spin-down* states. This behavior corresponds with the AFM arrangement of the Fe^{3+} magnetic moments. For YFO, the direct and indirect bandgaps energies are 3.29 and 3.08 eV, respectively. These values are large compared with the experimental reports, where YFO, for instance, has an estimated indirect band gap of 2.58 eV.[24] Meanwhile the *spin-up* and *spin-down* states of YFO-Bi show a direct bandgap of 2.88 eV and an indirect bandgap of 2.65 eV, respectively. In both cases, the character of the gap reflects the insulating or wide-semiconducting behavior of the compounds, such response is comparable to that observed in $BiFeO_3$, where the theoretical and experimental bandgap have been reported from 2.64 to 2.74 eV.[25-27]

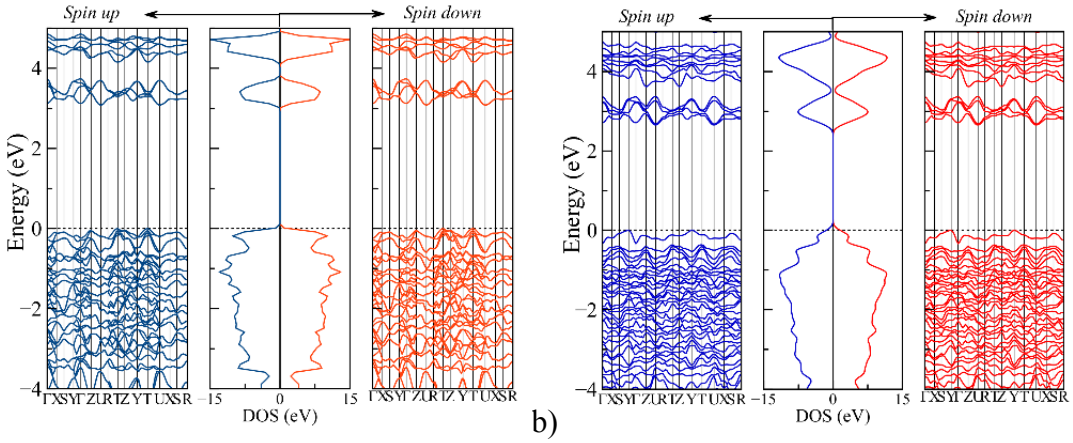

Figure 2. Band structure (TDOS in the center part of the Figure) obtained for (a) YFO and (b) YFO-Bi.

To identify the polar effects that bismuth produces in the YFO matrix, we perform spontaneous polarization calculations based on the modern polarization theory.[16,17] To calculate the spontaneous polarization (**P**s), we use an orthorhombic perovskite centrosymmetric structure (space group No. 62, *Pnma*) as a reference cell ($\lambda = 0$)[28]; starting from it, its evolution was followed until the distorted structure ($\lambda = 1$) of the YFO-Bi was reached. Finally, the spontaneous polarization can be expressed as, **P**s = $\mathbf{P}_{(\lambda = 1)} - \mathbf{P}_{(\lambda = 0)}$ for the YFO-Bi compound. **P**s was evaluated along the [100], [010], [001] and [101] directions of YFO-Bi. As shown in Figure 3, the largest change in **P**s is found along the [101] direction. In the undistorted structure ($\lambda = 0$), **P**s is 0.73 μC/cm^2 in the [101] direction; this contribution might stem from the imbalance of electronic clouds introduced by Bi-6*s*. For the post-structural relaxation, a maximum **P**s of 10.39 μC/cm^2 along [101] was obtained, a value that is higher than the experimental value reported for a YFO film with a remnant polarization of about 0.07 μC/cm^2,[29] and is lower compared with the calculated spontaneous polarization value of ∽91 μC/cm^2 for $BiFeO_3$ compound.[30] This is due to the breaking of some Y-O bonds because of the substitution of Bi at the Y site and the formation of new Bi-O bonds. A relative displacement of ions is produced with respect to the length of the Y-O bonds of the pure YFO, especially on the (040) plane (see Figures 4 and 5A Additionally, Figure 5B shows the electron localization function (ELF) projected on the (040) plane for YFO-Bi. A small charge density can be seen shared between the O^{2-} and the Bi^{3+}/Y^{3+}. An asymmetric distribution of the charges around the Bi ions is observed as a result of the Bi-6*s* electrons. Such

asymmetric distribution gives rise to **P**s values similar to those reported in previous works.[30]

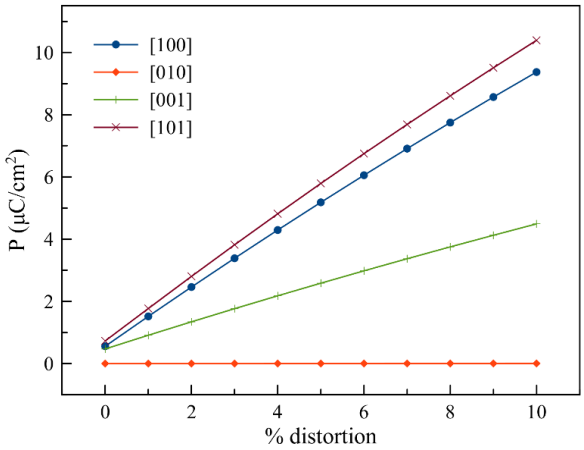

Figure 3. Change in polarization along a path from the centrosymmetric orthorhombic *Pmna* structure to the final distorted structure of YFO-Bi.

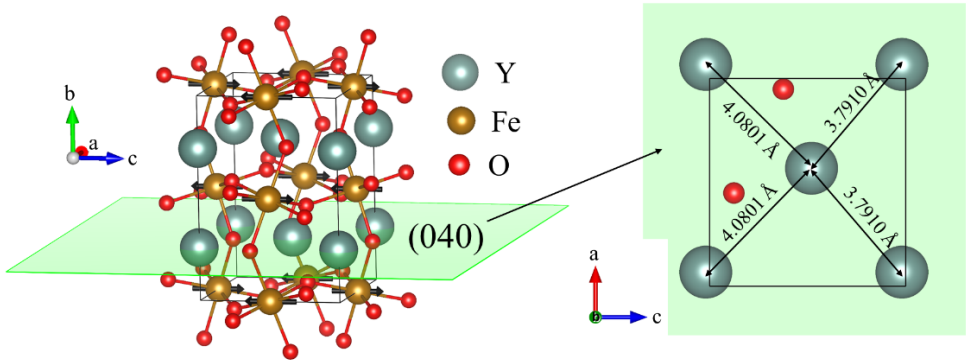

Figure 4. Analysis of the structural distortion in the (040) plane of YFO.

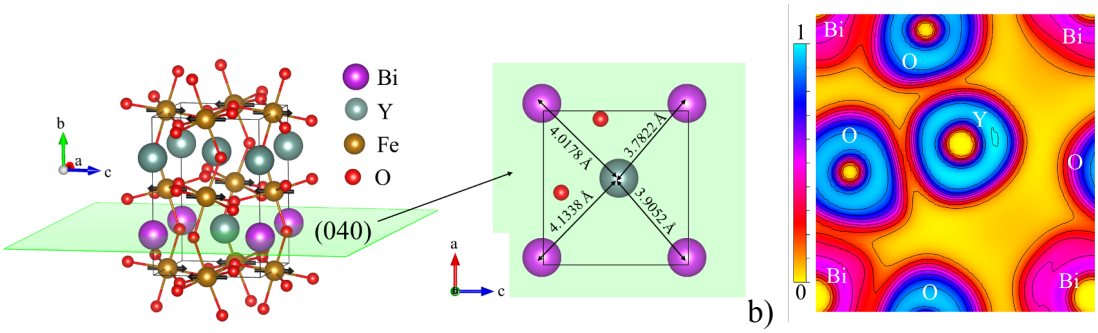

a) b)

Figure 5. a) Analysis of the structural distortion produced by the incorporation of the Bi ion and b) ELF projected in the (040) plane of YFO-Bi.

The optical response of Bi^{3+} doped YFO were derived from the dielectric function where the imaginary part is associated with the electronic transitions from the occupied states of the valence band to the unoccupied states of the conduction band. On other hand, the complex index of refraction $N(\vec{q},\omega)$ is associated with the dielectric function

by $N = \varepsilon^{1/2}$, that is, $N(\vec{q}, \omega) = \varepsilon_r + i\varepsilon_i$, where N can be written as $N = n + ik$, where n is the index of refraction and k is the extinction coefficient.[18] From this association it is possible to determine the refractive index and the extinction coefficient of the medium by

$$n = \left[\frac{\varepsilon_r}{2} + \frac{1}{2}(\varepsilon_r{}^2 + \varepsilon_i{}^2)^{\frac{1}{2}}\right]^{\frac{1}{2}} \quad (4)$$

$$k = \left[-\frac{\varepsilon_r}{2} + \frac{1}{2}(\varepsilon_r{}^2 - \varepsilon_i{}^2)^{\frac{1}{2}}\right]^{\frac{1}{2}} \quad (5)$$

To facilitate interpretation, we use ε as a function of energy, thus, the real ($\varepsilon_r(E)$) and imaginary ($\varepsilon_i(E)$) parts of YFO and YFO-Bi are shown in Figure 6a) and b), respectively. This graph shows an increase in the static dielectric constant ($\varepsilon_r(0)$), from 5.88 (Figure 6a)) for YFO to 6.42 (Figure 6b)) for YFO-Bi, so that the electric polarizability is increased when Bi is incorporated into the YFO system. On the other hand, in YFO, the three components of $\varepsilon_i(E)$, $\varepsilon_{ixx}, \varepsilon_{iyy}, \varepsilon_{izz}$, are approximately equal up to ~3 eV (Figure 6a). For higher photon energies each component behaves differently due to the interaction between Fe-3*d* and Y-4*d* above the fermi level and O-2*p* states in the valence band (see Figure. S2 in supplementary material). Thus, for values greater than 3 eV, we can consider the YFO compound as a biaxial crystal that exhibits two effective refractive indices different from the individual principal values. In the case of YFO-Bi, the $\varepsilon_i(E)$ graphs show $\varepsilon_{iyy} = \varepsilon_{izz}$, up to ~5 eV, while ε_{ixx} starts with the same value but departs from it at around 2.5 eV taking higher values. Additionally, a more detailed analysis of the tensorial components of the dielectric function, real (Figure 6c)) and imaginary parts (Figure 6d)) are shown for YFO-Bi. It becomes clear that components $\varepsilon_{r\,xz}(E)$ and $\varepsilon_{r\,zx}(E)$ are the more significant, while the other components contribute to a lesser extent (Figure 6c)). Similarly, the same happens for the imaginary part where functions $\varepsilon_{i\,xz}(E)$ and $\varepsilon_{i\,zx}(E)$ are more significant (Figure 6d)). Whence, it becomes evident that there is an anisotropic polarizability in the [101] direction, coinciding with that where the maximum spontaneous polarization, previously discussed, is found.

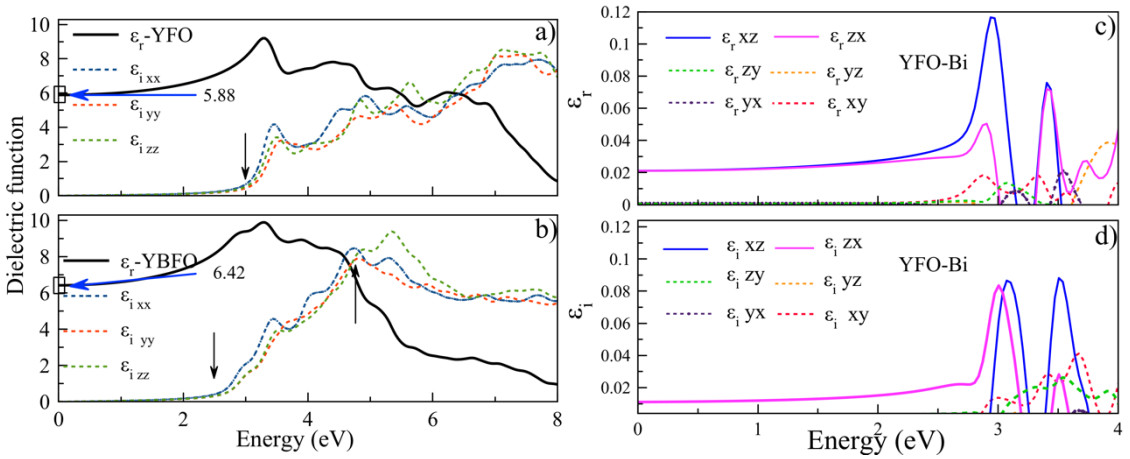

Figure 6. Calculated components of the permittivity of a) YFO and b) YBFO. In c) the non-diagonal components of the real part of the ε_r tensor, $\varepsilon_{r\,xy}$, $\varepsilon_{r\,xz}$, $\varepsilon_{r\,yx}$, $\varepsilon_{r\,zx}$, $\varepsilon_{r\,zy}$ and $\varepsilon_{r\,yz}$ are shown. In d) the imaginary components of the dielectric function are displayed. Solid lines indicate the components of greater magnitude.

Finally, the refractive index (n) and extinction coefficient (k) quantities are shown in Figure 7. The behavior of k indicates that with the incorporation of Bi, the material absorbs energies above 2 eV, while for the compound YFO, this occurs above 3 eV, which is consistent with the gap values obtained in the DOS. In particular, the Bi^{3+} ion in the YFO matrix (dashed line YFO-Bi_k) produces a sharp increase of k to an energy value a bit lower than that of YFO, This may be due to the electrons present in the orbital 6*s* of Bi ion and 3*d* in Fe ion at energies close to 2.5 eV (see Figure S1b in supplementary material), while there is a sudden increase above 3.1 eV for the YFO. The variation of refractive index vs. photon energy is shown in Figure 7. At 0 eV energy, the value of n is found to be ∽2.42 for YFO and ∽2.53 for YFO-Bi, their maximum value is in the UV region with $n_{max} = 3.05$ for YFO and $n_{max} = 3.18$ for YFO-Bi. These values are comparable with those of the $BiFeO_3$, where n_{max} is ∽3.3[26]; from the above, we deduce that the introduction of Bi in the YFO matrix favors the increase of the n value. This is caused by the Bi-6*s* and Bi-6*p* states above 2.5 eV in the conduction band.

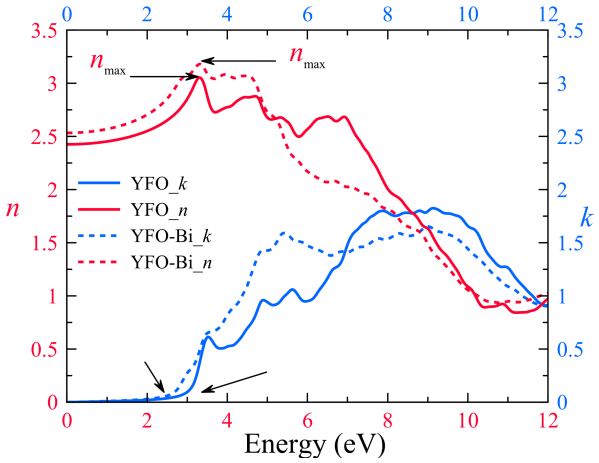

Figure 7. Refractive index and extinction coefficient of YFO and BYFO.

4. Conclusions

In this study, we have determined the ferroelectric, magnetic and optical properties of $YFeO_3$ and $Y_{0.75}Bi_{0.25}FeO_3$, using first-principles calculations based on DFT. In both compounds, the G-type antiferromagnetic configuration was established as the most stable, along with a magnetization of Fe equal to ±4.03 μB. The lattice parameters of YFO-Bi are larger than those of YFO due to the larger ionic radius of Bi, which also produces a distortion of the YO_6 and BiO_6 octahedra. The Bi^{3+} ion reduces the bandgap, from 3.29 eV (YFO) to 2.88 eV (YFO-Bi), establishing the latter compound as a narrow bandgap material. Our calculations have revealed that the spontaneous polarization of YFO-Bi in the [101] direction is 10.39 μC/cm^2, which opens the door for the use of this material for ferroelectric applications.

Furthermore, the optical properties were determined by means of the complex dielectric function, from which an increase of $\varepsilon_r(0)$, from 5.88 (YFO) to 6.42 (YFO-Bi) was observed. Finally, we determined that the highest ε_r is observed for the ε_{rxz} and ε_{rzx} tensorial components, which are associated with the same direction along which the spontaneous polarization of YFO-Bi occurs.

Acknowledgments

The authors thank the computer support thorough Projects LANCAD-UNAM-DGTIC-351. E. Martínez-Aguilar thanks PRODEP-SEP, Mexico for scholarship grant No. 511-

6/2020.-2176. J. M. Siqueiros acknowledges the support of DGAPA-UNAM through Project IN104320.

References

[1] G. Catalan, J. F. Scott, Adv. Mater. 2009, 21, 2463.
[2] S. Bipul Deka, A. P. Ravi, D. Pamu, Ceram. Int. 2017, 43, 1323.
[3] M. Wang, T. Wang, S.-H. Song, M. Ravi, R.-C. Liu, S.-S. Ji, Ceram. Int. 2017, 43, 10270.
[4] M. Shang, C. Zhang, T. Zhang, L. Yuan, L. Ge, H. Yuan, S. Feng, Appl. Phys. Lett. 2013, 102, 062903.
[5] M. Wang, T. Wang, S. Song, M. Tan, Materials 2017, 10, 626.
[6] K. T. Jacob, G. Rajitha, N. Dasgupta, Indian J. Eng. Mater. Sci. 2012, 19, 47.
[7] X. Yuan, Y. Sun, M. Xu, J. Solid State Chem. 2012, 196, 362.
[8] A. M. Bolarín-Miró, F. Sánchez-De Jesús, C. A. Cortés-Escobedo, R. Valenzuela, S. Ammar, J. Alloys Compd. 2012, 586, S90 –, 2014. SI: ISMANAM.
[9] S. Madolappa, B. Ponraj, R. Bhimireddi, K. B. R. Varma, J. Am. Ceram. Soc. 2017, 100, 2641.
[10] O. Rosales-González, F. Sánchez-De Jesús, F. Pedro-García, C. A. Cortés-Escobedo, M. Ramírez-Cardona, A. M. Bolarín-Miró, Materials 2019, 12, 2054.
[11] Z. Zhang, P. Wu, L. Chen, J. Wang, Appl. Phys. Lett. 2010, 96, 012905.
[12] J. Kaczkowski, Comput. Mater. Sci. 2018, 152, 183.
[13] P. Giannozzi, S. Baroni, N. Bonini, M. Calandra, R. Car, C. Cavazzoni, G. L. Davide Ceresoli, M. C. Chiarotti, I. Dabo, A. D. Corso, S. de Gironcoli, S. Fabris, G. Fratesi, R. Gebauer, U. Gerstmann, C. Gougoussis, A. Kokalj, M. Lazzeri, L. Martin-Samos, N. Marzari, F. Mauri, R. Mazzarello, S. Paolini, A. Pasquarello, L. Paulatto, C. Sbraccia, S. Scandolo, G. Sclauzero, A. P. Seitsonen, A. Smogunov, P. Umari, R. M. Wentzcovitch, J. Phys.: Condens. Matter 2009, 21, 395502.
[14] A. M. Rappe, K. M. Rabe, E. Kaxiras, J. D. Joannopoulos, Phys. Rev. B 1990, 41, 1227.
[15] N. J. Ramer, A. M. Rappe, Phys. Rev. B 1999, 59, 12471.
[16] R. D. King-Smith, D. Vanderbilt, Phys. Rev. B 1993, 47, 1651.
[17] D. Vanderbilt, R. D. King-Smith, Phys. Rev. B 1993, 48, 4442.
[18] T. Wolfram, S. Ellialtioglu, Electronic and Optical Properties of d-Band Perovskites, Cambridge University Press, Middle East Technical University, Ankara, Turkey 2006.
[19] D. du Boulay, E. N. Maslen, V. A. Streltsov, N. Ishizawa, Acta Crystallogr. Sect. B 1995, 51, 921.
[20] R. D. Shannon, Acta Crystallogr. Sect. A 1976, 32, 751.
[21] Y. Sui, C. Xin, X. Zhang, Y. Wang, Y. Wang, X. Wang, Z. Liu, B. Li, X. Liu, J. Alloys Compd. 2015, 645, 78.
[22] T. Shen, C. Hu, W. L. Yang, H. C. Liu, X. L. Wei, Mater. Sci. Semicond. Process. 2015, 34, 114.
[23] M. K. Warshi, V. Mishra, V. Mishra, R. Kumar, P. R. Sagdeo, Ceram. Int. 2018, 44, 13507 – 13512.
[24] M. A. Butler, D. S. Ginley, M. Eibschutz, J. Appl. Phys. 1977, 48, 3070.
[25] E. Martínez-Aguilar, H. H'Mok, M. G. Moreno-Armenta, J. M. Siqueiros, Ferroelectrics 2018, 535, 82.
[26] J.-P. Xu, R.-J. Zhang, Z.-H. Chen, Z.-Y. Wang, F. Zhang, X. Yu, A.-Q. Jiang, Y.-X. Zheng, S.-Y. Wang, L.-Y. Chen, Nanoscale Res. Lett. 2014, 9, 188.

[27] J. F. Ihlefeld, N. J. Podraza, Z. K. Liu, R. C. Rai, X. Xu, T. Heeg, Y. B. Chen, J. Li, R. W. Collins, J. L. Musfeldt, X. Q. Pan, J. Schubert, R. Ramesh, D. G. Schlom, Appl. Phys. Lett. 2008, 92, 142908.
[28] R. Resta, D. Vanderbilt, Topics in Applied Physics of Ferroelectrics, (Eds: Topics in Applied Physics), Vol. 105, Springer, Berlin, Heidelberg 2007.
https://doi.org/10.1007/978-3-540-34591-6_2.
[29] R.-L. Zhang, C.-L. Chen, Y.-J. Zhang, H. Xing, X.-L. Dong, K.-X. Jin, Chin. Phys. B 2015, 24, 017701.
[30] H. H'Mok, E. Martínez Aguilar, J. Antúnez García, J. Ribas Ariño, L. Mestres, P. Alemany, D. H. Galván, J. M. Siqueiros Beltrones, O. Raymond Herrera, Comput. Mater. Sci. 2019, 164, 66.